Acoustic plasmons in extrinsic free-standing graphene

2014 New J. Phys. 16 083003

(http://iopscience.iop.org/1367-2630/16/8/083003)

New Journal of Physics
The open access journal at the forefront of physics
Deutsche Physikalische Gesellschaft DPG | IOP Institute of Physics

Acoustic plasmons in extrinsic free-standing graphene

M Pisarra[1], A Sindona[1], P Riccardi[1], V M Silkin[2,3,4] and J M Pitarke[5,6]

[1] Dipartimento di Fisica, Università della Calabria and INFN—Gruppo collegato di Cosenza, Via P Bucci cubo 30 C, 87036 Arcavacata di Rende (CS), Italy
[2] Donostia International Physics Center, Paseo Manuel de Lardizabal 4, E-20018 Donostia-San Sebastian, Basque Country, Spain
[3] Departamento de Física de Materiales, Facultad de Ciencias Químicas, UPV/EHU, Apartado 1072, E-20080 Donostia-San Sebastian, Basque Country, Spain
[4] IKERBASQUE, Basque Foundation for Science, 48011 Bilbo, Basque Country, Spain
[5] CIC nanoGUNE, Tolosa Hiribidea 76, E-20018 Donostia-San Sebastian, Basque Country, Spain
[6] Materia Kondentsatuaren Fisika Saila and Centro Fisica Materiales CSIC-UPV/EHU, 644 Posta Kutxatila, E-48080 Bilbo, Basque Country, Spain
E-mail: michele.pisarra@fis.unical.it

Received 14 April 2014
Accepted for publication 10 June 2014
Published 4 August 2014

New Journal of Physics **16** (2014) 083003

doi:10.1088/1367-2630/16/8/083003

Abstract

An acoustic plasmon is predicted to occur, in addition to the conventional two-dimensional (2D) plasmon, as the collective motion of a system of two types of electronic carriers coexisting in the same 2D band of *extrinsic* (doped or gated) graphene. The origin of this novel mode stems from the anisotropy present in the graphene band structure near the Dirac points K and K′. This anisotropy allows for the coexistence of carriers moving with two distinct Fermi velocities along the ΓK and ΓK′ directions, which leads to two modes of collective oscillation: one mode in which the two types of carriers oscillate in phase with one another (this is the conventional 2D graphene plasmon, which at long wavelengths ($q \to 0$) has the same dispersion, $q^{1/2}$, as the conventional 2D plasmon of a 2D free electron gas), and the other mode found here corresponds to a low-frequency acoustic oscillation (whose energy exhibits at long-wavelengths a linear dependence on the 2D wavenumber q) in which the two types of carriers oscillate out of phase. This prediction represents a realization of acoustic

plasmons originated in the collective motion of a system of two types of carriers coexisting within the same band.

Keywords: graphene, plasmons, time dependent DFT, linear response theory

In recent years, interest in graphene [1] has grown impressively for both fundamental research and technological applications [2–4]. This is due to the fact that graphene exhibits a number of interesting properties, related mainly to its *novel* electronic structure near the Fermi level, represented by the so-called Dirac cone. A major issue is represented in this case by the variation of the charge carrier density, which is caused by several conditions, including, for example, the shape and defects of graphene flakes, charge transfer processes with the supporting material [5], chemical doping [6, 7], and the application of gating potentials [1]. The appearance of a two-dimensional (2D) sheet plasmon in graphene adsorbed on a variety of supporting materials has been observed in several experiments [8–13], where monolayer graphene happens to be doped by charge transfer to or from the substrate. On the theoretical side, a number of calculations have have been able to reproduce a 2D sheet plasmon [14–24] in extrinsic (doped or gated) free-standing graphene.

In this paper, we present an *ab initio* description of the energy-loss spectrum of both intrinsic (undoped and ungated) and extrinsic free-standing monolayer graphene. Starting with pristine (intrinsic) graphene, we include the effect of electron injection by simply upshifting the Fermi level from the Dirac point, that is by working under the assumption that the graphene band structure is unaffected by doping. We find that the anisotropy that is present in the graphene band structure near the Dirac points K and K′ allows for the coexistence of a majority of carriers moving with two different velocities along the ΓK and ΓK′ directions, thus leading to a remarkable realization of the old idea [25] that low-energy acoustic plasmons (whose energy exhibits a linear dependence on the wavenumber) should exist in the collective motion of a system of two types of electronic carriers. Our energy-loss calculations, which we carry out in the random-phase approximation (RPA), show the existence of a low-frequency acoustic oscillation (in which the two types of carriers oscillate out of phase), in addition to the conventional 2D graphene collective mode described in [14, 15] (in which the two types of carriers oscillate in phase with one another).

We start with the following expression for the in-plane RPA complex dielectric matrix of a many-electron system consisting of periodically repeated (and well separated) graphene 2D sheets (atomic units are used throughout, unless stated otherwise):

$$\epsilon_{\mathbf{g},\mathbf{g}'}(\mathbf{q},\omega) = \delta_{\mathbf{g},\mathbf{g}'} - v_{\mathbf{g},\mathbf{g}'}(\mathbf{q}) \sum_{g_z,g_z'} \chi^0_{\mathbf{G},\mathbf{G}'}(\mathbf{q},\omega). \tag{1}$$

Here, $\mathbf{G} = (\mathbf{g}, g_z)$ is a three-dimensional (3D) reciprocal-lattice vector; $\mathbf{g}$ and $\mathbf{q}$ represent an in-plane 2D reciprocal-lattice vector and an in-plane first-Brillouin-zone (BZ) 2D wavevector, respectively; $v_{\mathbf{g},\mathbf{g}'}(\mathbf{q}) = 2\pi\delta_{\mathbf{g},\mathbf{g}'}/|\mathbf{q}+\mathbf{g}|$ denotes the 2D Fourier transform of the Coulomb potential; and

$$\chi^0_{\mathbf{G}\mathbf{G}'}(\mathbf{q},\omega) = \frac{2}{\Omega}\sum_{\mathbf{k}}^{\mathrm{BZ}}\sum_{v\,v'}\left(f_{v\mathbf{k}} - f_{v'\mathbf{k}+\mathbf{q}}\right)\frac{\left\langle v\mathbf{k}\middle|e^{-\mathrm{i}(\mathbf{q}+\mathbf{G})\cdot\mathbf{r}}\middle|v'\mathbf{k}+\mathbf{q}\right\rangle\left\langle v'\mathbf{k}+\mathbf{q}\middle|e^{\mathrm{i}(\mathbf{q}+\mathbf{G}')\cdot\mathbf{r}}\middle|v\mathbf{k}\right\rangle}{\omega + \varepsilon_{v\mathbf{k}} - \varepsilon_{v'\mathbf{k}+\mathbf{q}} + \mathrm{i}\eta} \tag{2}$$

represents the 3D Fourier transform of the density response function of non-interacting electrons confined to a normalization volume Ω and occupying the band states $|v\mathbf{k}\rangle$, $|v'\mathbf{k}+\mathbf{q}\rangle$, with energies $\varepsilon_{v\mathbf{k}}$, $\varepsilon_{v'\mathbf{k}+\mathbf{q}}$, and occupation factors $f_{v\mathbf{k}}$, $f_{v'\mathbf{k}+\mathbf{q}}$, $\mathbf{k}$ being an in-plane 2D wavevector in the first BZ. These states and energies are the eigenvectors and eigenvalues of a single-particle Hamiltonian, which we take to be the Kohn–Sham (KS) Hamiltonian of density functional theory (DFT).

The inelastic scattering cross section corresponding to a process in which (after the scattering of external electrons or electromagnetic waves) an electronic excitation of wavevector $\mathbf{q}+\mathbf{g}$ and energy ω created at the graphene 2D sheet is proportional to the energy-loss function $\mathrm{Im}\,[-\epsilon^{-1}_{\mathbf{g},\mathbf{g}}(\mathbf{q},\omega)]$. Collective excitations (plasmons) are dictated by the zeros in the real part of the macroscopic dielectric function

$$\epsilon_M(\mathbf{q}+\mathbf{g},\omega)=\frac{1}{\epsilon^{-1}_{\mathbf{g},\mathbf{g}}(\mathbf{q},\omega)} \tag{3}$$

in an energy region where the imaginary part is small.

Our *ab initio* scheme begins with the KS eigenvalues and eigenvectors, which we calculate in the local-density approximation (LDA) by using the Perdew–Zunger parametrization [26] of the uniform-gas correlation energy. We use a plane-wave basis set (with a cut-off energy of 25 Hartrees) and a norm-conserving pseudopotential of the Troullier–Martins type [27]. Our system is made using periodically repeated 2D graphene sheets separated by a distance of ∼40 a.u. The BZ integration is carried out using an unshifted $60\times60\times1$ Monkhorst–Pack grid [28], which results in a 3600 $\mathbf{k}$-point sampling of the BZ. From the converged electron density, we calculate the KS single-particle energies and orbitals on a denser $\mathbf{k}$-point mesh ($720\times720\times1$) including up to 60 bands. These KS energies and orbitals are plugged into equation (2), which we use to obtain the χ^0 matrix with up to ∼500 $\mathbf{G}$-vectors. The in-plane RPA complex dielectric matrix is then computed from equation (1). For the wavevectors and energies of interest here (below the π plasmon at ∼5 eV), stable results were obtained by including in equation (2) 51 reciprocal-lattice vectors of the form $\mathbf{G}=\{0,g_z\}$.

In the case of *intrinsic* graphene, the calculated energy-loss function presents three well-known distinct features. First of all, there is a broad peak-like structure starting at low values of q and ω (see figure 1), which originates at interband $\pi\rightarrow\pi^*$ single-particle (SP) excitations [14, 15] and was erroneously interpreted as a *cone plasmon* in [22]. Second, there is the π plasmon (πP) starting at ∼5 eV (see figure 1) (also present in graphite [29]), which in the case of monolayer graphene is red-shifted and exhibits a linear dispersion [30, 31] distinct from the parabolic dispersion in graphite. Third, there is the broad high-energy graphene $\sigma-\pi$ plasmon peak starting at ∼15 eV (not visible in figure 1), which corresponds to the graphite $\sigma-\pi$ plasmon at ∼27 eV [32].

For *extrinsic* graphene, we adjust the occupation factors of equation (2) to account for positive Fermi-energy shifts $\Delta E_F=0.5$ eV and $\Delta E_F=1.0$ eV relative to the Dirac point, corresponding to charge-carrier densities of 2.36×10^{13} cm^{-2} and 1.15×10^{14} cm^{-2}, respectively[7]. Figure 2 exhibits a comparison of the RPA energy-loss function that we have

[7] Charge-carrier densities achievable with gating potentials are typically of the order of 10^{12}–10^{13} cm^{-2} [1]. Higher doping levels can be achieved through chemical doping; indeed, a displacement of the Fermi level as high as ∼2 eV, with respect to the Dirac point, has been achieved after the intercalation of alkali metals on supported graphene [7].

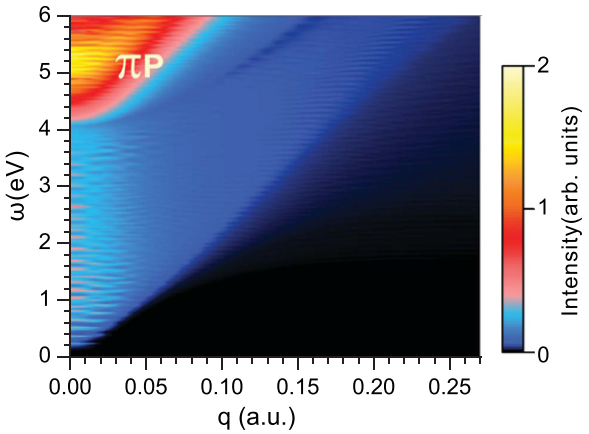

Figure 1. 2D plot of the energy-loss function of *intrinsic* graphene vs the magnitude of the in-plane wavevector **q** along the ΓK direction (horizontal axis) and the energy ω (vertical axis).

obtained along the ΓK and ΓM directions. This doping affects neither the π nor the σ-π plasmon. Important differences are visible, however, at low q and ω, where we can identify the opening of a gap in the SP excitation spectrum of *extrinsic* graphene. More importantly, two collective modes (plasmons) are clearly visible in the case of *extrinsic* graphene (which are absent in *intrinsic* graphene): (i) the conventional graphene 2D plasmon (2DP) [14, 15], which within the gap (of the SP excitation spectrum) has no damping (and exhibits the same dispersion, $q^{1/2}$, as the conventional plasmon of a 2D electron gas [33]) and outside the gap has a finite linewidth, and (ii) a well-defined low-frequency mode (the *new* acoustic plasmon, AP), whose energy exhibits at long wavelengths ($q \to 0$) a linear dependence on q. Figure 2 shows that while the 2DP mode is present along both directions ΓK and ΓM, the AP mode is present only along ΓK; this figure also shows that the energy dispersion of the *acoustic* plasmon strongly depends on the doping level.

In order to demonstrate that the energy-loss peaks that are visible in figure 2 correspond to collective excitations, we have plotted in figure 3 the energy-loss function (red dotted line) for a given value of q (q = 0.09 a.u.) and ΔE = 1.0 eV, together with the real (black solid line) and the imaginary (green dashed line) parts of the macroscopic dielectric function ϵ_M of equation (3). This figure shows that Re $[\epsilon_M]$ exhibits *two* distinct zeros (marked by the open circles I and II) in energy regions where Im ϵ_M is small and the energy-loss function is, therefore, large. These two zeros (*each* of them being associated to the *two* maxima B1 and B2 in Im $[\epsilon_M]$) represent a signature of well-defined collective excitations: (i) the higher-energy plasmon (the conventional graphene 2D plasmon, 2DP) occurs at an energy (just above the upper edge $v_F\, q$ of the intraband SP excitation spectrum, v_F being the graphene Fermi velocity) where only interband SP excitations are possible. (ii) The low-energy plasmon (the *new* acoustic plasmon, AP) occurs at an energy that stays below $\omega = v_F\, q$, so it is damped through intraband SP excitations; nonetheless, Im $[\epsilon_M]$ is still considerably small at this energy, which confirms that this low-energy mode represents a well-defined collective excitation as well.

The existence of the low-energy acoustic plasmon could not possibly have been anticipated in the framework of the so-called 'Dirac-cone approximation' [14, 15], simply because an oversimplified isotropic graphene band structure was considered in the vicinity of

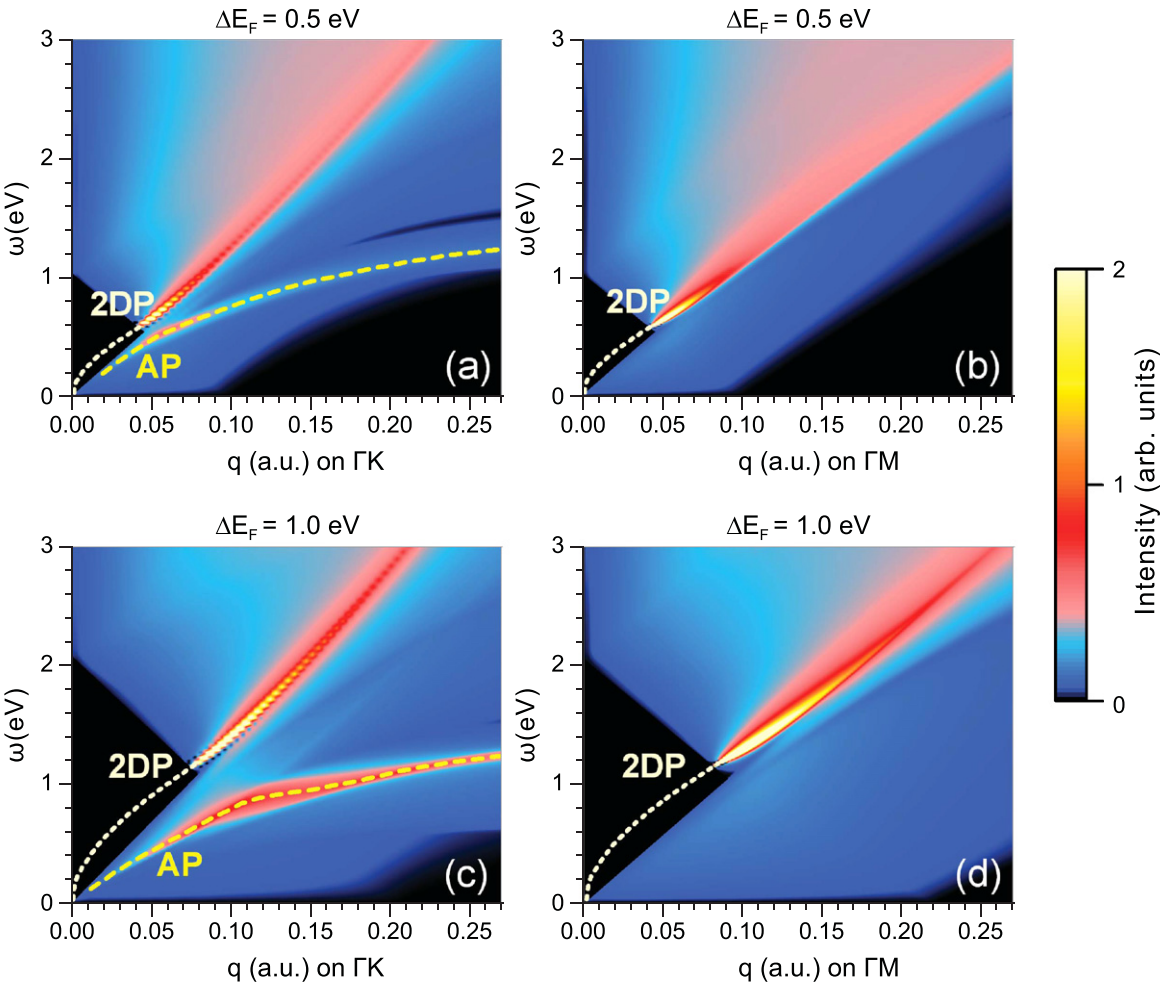

Figure 2. 2D plot of the energy-loss function of *extrinsic* graphene vs the magnitude of the in-plane wavevector **q** (along the (a, c) ΓK and (b, d) ΓM directions) (horizontal axis) and the energy ω (vertical axis). The Fermi level has been shifted (a, b) 0.5 eV and (c, d) 1.0 eV above the Dirac point. The dotted lines represent the energy dispersion of the conventional 2D plasmon (2DP), as obtained from the zeros of the real part of the macroscopic dielectric function [ϵ_M]. The dashed lines simply highlight the energy dispersion of the acoustic plasmon (AP).

the K-point. A signature of such a mode has been detected recently [22–24]; but it was erroneously interpreted in [22] as a nonlinear mode along the nonlinear branch of the cone structure, and it was not discussed in [23, 24].

With the aim of revealing the origin of the low-energy acoustic plasmon (the *new* plasmon), we show in figure 4: (i) the dispersion of the graphene π and π^* bands along various high-symmetry paths originating at the K point (figure 4(a)) and (ii) the density-of-states distribution in these bands (figures 4(b), (c)). The graphene π and π^* energy dispersions are plotted in figure 4(a) along the K Γ and KM branches in the ΓK direction, and along the KK branch in the ΓM direction, together with the isotropic energy dispersion that is obtained in the Dirac-cone approximation.

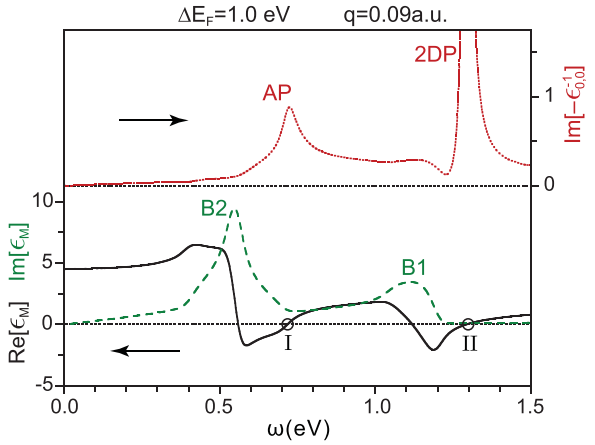

Figure 3. The energy-loss function Im $[-\epsilon^{-1}_{\mathbf{0},\mathbf{0}}(\mathbf{q}, \omega)]$ (red dotted line), Re $[\epsilon_M(\mathbf{q}, \omega)]$ (black solid line), and Im $[\epsilon_M(\mathbf{q}, \omega)]$ (green dashed line) of *extrinsic* graphene ($\Delta E_F = 1.0$ eV) vs the energy ω for a fixed value of the magnitude of $\mathbf{q}$ ($q = 0.09$ a.u.) along the ΓK direction.

The band-structure anisotropy that is visible in figure 4(a) implies the unique behavior of the density of states shown in figures 4(b) and (c) as a function of the single-particle energy E and the group velocity (see footnote 8). Along the ΓM direction (figure 4 (c)) the density of states is peaked (at the energies of interest, i.e., below ∼1.5 eV) around one single Fermi velocity $v_F \sim 1 \times 10^6$ m s^{-1} (peak B1 above the Dirac point and peak B1′ below), as occurs in a free-electron gas. On the other hand, the density of states along the ΓK direction (figure 4 (b)) is peaked at two distinct velocities (peaks B1 and B2 above the Dirac point, and B1′ and B2′ below) within the very same band. Since for a low wavevector along a given direction the number of allowed intraband transitions—dictated by Im $[\epsilon_M]$—is known to be proportional to the density of states with group velocity along that direction [35], we conclude that intraband transitions along the ΓK direction happen to be determined by the coexistence of carriers moving with two distinct Fermi velocities, yielding the maxima B1 and B2 in figure 3. This leads to two modes of collective oscillation: (i) one mode (the conventional 2D plasmon, 2DP) in which the two types of carriers oscillate in phase with one another with an energy that is along ΓK slightly larger than along ΓM (where only one type of carriers participate and the 2DP dispersion—outside the gap—simply follows the upper intraband edge v_{Fq} [14, 15]), and (ii) another mode (the *new* acoustic plasmon, AP) which corresponds to an *acoustic* oscillation of lower frequency in which the two types of carriers residing in branches B1 (B1′) and B2 (B2′) oscillate out of phase.

Hence, hereby we shed light on the observed deviation (along the ΓK direction) of the 2DP dispersion curve towards energies that are (outside the gap) above the upper intraband edge v_{Fq} [9]. And hereby we predict the existence (along the ΓK direction) of a remarkable *acoustic* plasmon as the collective motion of a system of two types of electronic carriers coexisting in the very same 2D band of *extrinsic* graphene.

The complete anisotropic dispersion of both plasmons (2DP and AP) is shown in figures 5 and 6, respectively, where the plasmon energy is plotted vs the in-plane 2D wavevector $\mathbf{q}$. Figure 5 clearly shows that the conventional 2D plasmon dispersion is (i) isotropic at wavevectors below ∼0.05 a.u., where neither intraband nor interband transitions are available

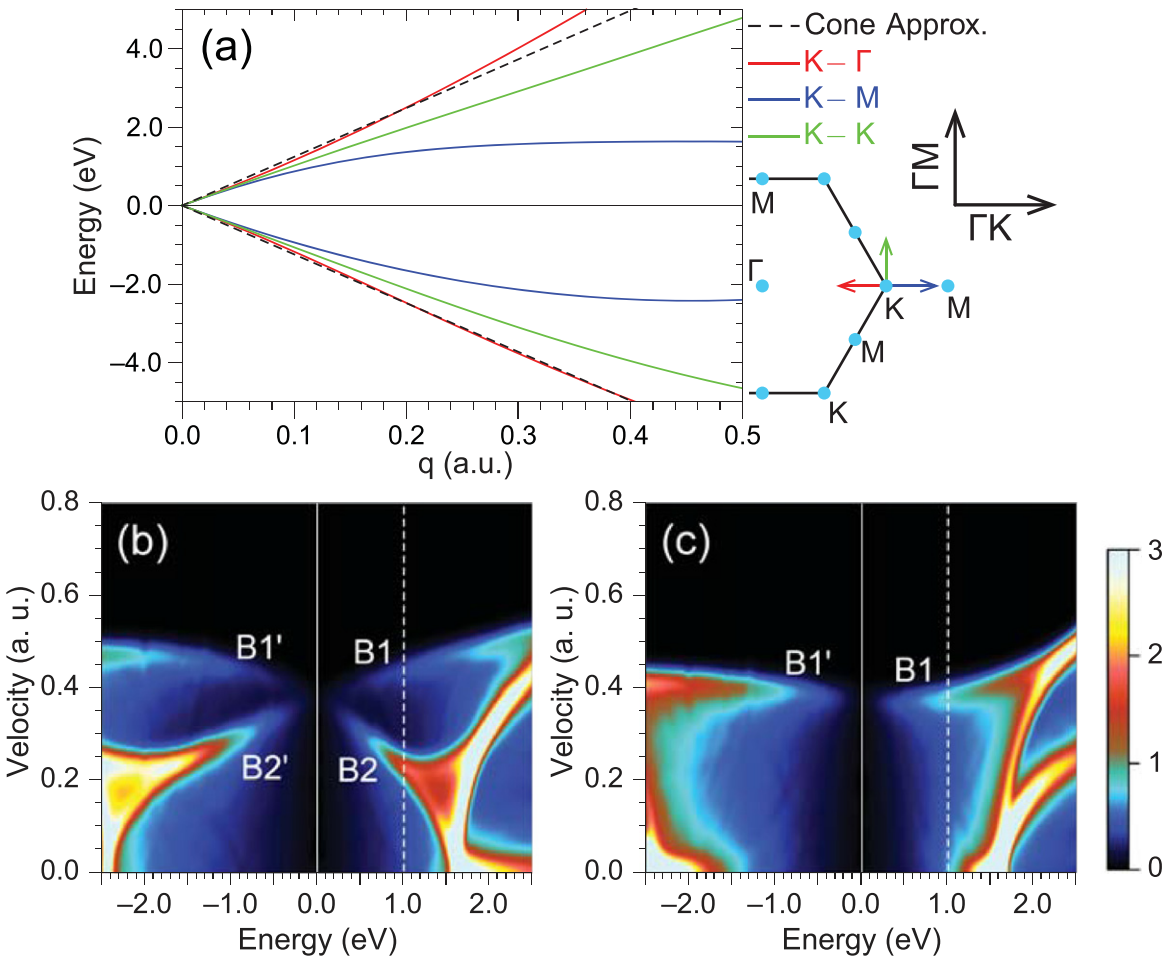

Figure 4. (a) The graphene DFT band structure in the vicinity of the K point, as obtained along three high-symmetry paths: the KΓ and KM branches (red and blue lines, respectively) in the ΓK direction, and the KK branch (green line) in the ΓM direction; the Dirac-cone approximation is represented by a black dashed line. Partial density of states along (b) ΓK and (c) ΓM vs the single-particle energy E and the group velocity[8]. The solid and dashed vertical lines represent the Fermi level of *intrinsic* graphene and *extrinsic* graphene (with $\Delta E_F = 1$ eV), respectively.

and there is no damping, and (ii) anisotropic at larger wavevectors (reflecting the 6-fold symmetry of the graphene BZ) with the plasmon energy being along the ΓK direction larger than along the ΓM direction (as discussed above).

Figure 6 shows that the *new* acoustic plasmon exhibits a remarkable anisotropy. At small wavevectors, the energy of the AP increases linearly with the magnitude of the wavevector, with a slope that is minimum along the ΓK direction and increases as one moves away from that direction until the AP completely disappears at wavevectors **q** along the ΓM direction (grey

[8] We define the group velocity for each band n as $\mathbf{v}_n = \nabla_{\mathbf{k}} \varepsilon_n(\mathbf{k})$ [34], where $\varepsilon_n(\mathbf{k})$ represents the energy dispersion of the nth band. The partial density of states is then readily calculated by 'counting' the number of states with a given energy E and velocity $v_{\hat{\imath}}$ in the $\hat{\imath}$-direction. By integrating over $v_{\hat{\imath}}$, the conventional density of state is obtained as a function of E.

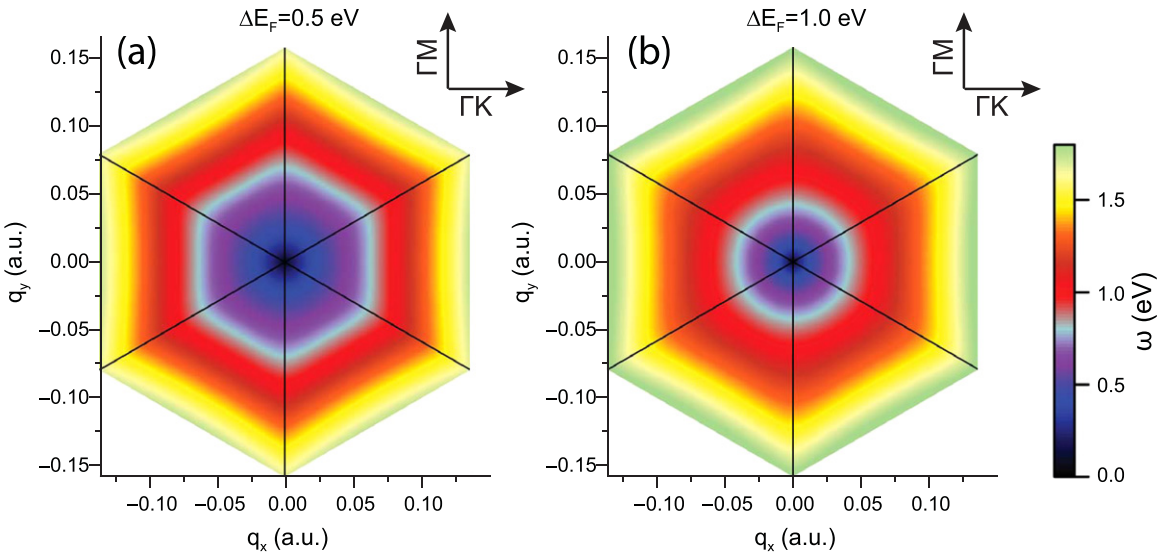

Figure 5. Energy (in eV) of the conventional 2D plasmon (2DP) of extrinsic graphene vs the in-plane 2D wavevector **q**. The Fermi level has been shifted (a) 0.5 eV and (b) 1.0 eV above the Dirac point.

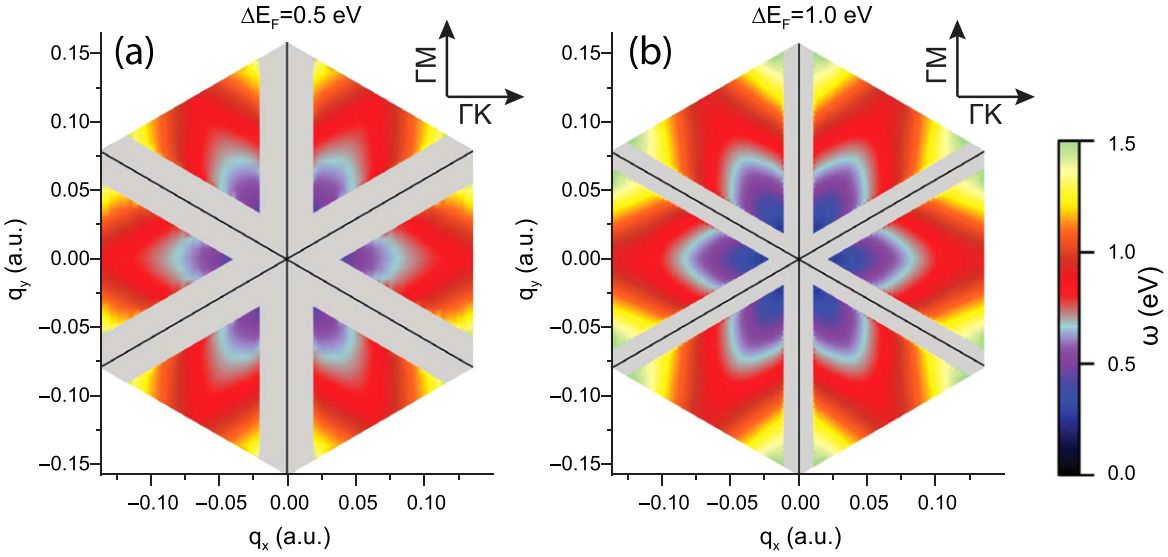

Figure 6. Energy (in eV) of the acoustic plasmon (AP) of extrinsic graphene vs the in-plane 2D wavevector **q**. The Fermi level has been shifted (a) 0.5 eV and (b) 1.0 eV above the Dirac point. The grey color shows regions where the AP is not found to exist. For the **k** mesh and numerical broadening used in our calculations, we have been able to trace the existence of the graphene AP down to $\omega \approx 0.2$ eV and $\omega \approx 0.1$ eV for $\Delta E_F = 0.5$ eV and $\Delta E_F = 1.0$ eV, respectively.

areas). Since, as seen in figure 4(b), the Fermi velocity in branches B2 and B2′ strongly depends on the position of the Fermi level, the initial slope of the AP dispersion (determined by the corresponding Fermi velocity [36]) significantly changes upon variation of the doping, as one can appreciate from comparison of figures 2 (a) and (c). We also note that, since the density-of-

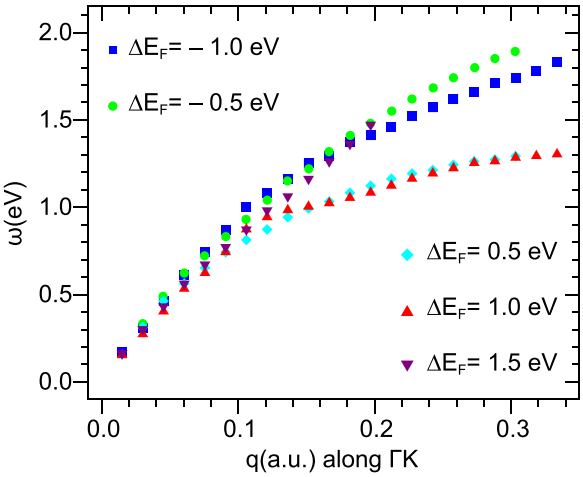

Figure 7. Energy dispersion of the graphene AP plasmon along the ΓK direction, for various values of the doping.

states double-peak structure is present also below the Dirac point, the AP plasmon should occur for *p*-doping as well. Indeed, we have found that the AP is also present for negative ΔE_F. In figure 7 we show the AP energy dispersion along the ΓK direction for various values of the doping, both *p*-doping ($\Delta E_F < 0$) and *n*-doping ($\Delta E_F > 0$). We clearly see that, notwithstanding the different doping values, the AP mode shows a linear dispersion in the $q \to 0$ limit.

In summary, we have demonstrated that as a consequence of the fact that two types of carriers in *extrinsic* graphene (moving with two distinct Fermi velocities) coexist within the very same 2D band, (i) the conventional 2D plasmon (corresponding to the two types of carriers oscillating in phase with one another) disperses along the ΓK direction with an energy that is higher than along the ΓM direction, and (ii) there is an additional *acoustic* plasmon (corresponding to the two types of electrons oscillating out of phase). Low-energy acoustic plasmons are known to exist [36–45] at metal surfaces where a two-component scenario (one component consisting of a quasi 2D surface-state band and the other component being the underlying bulk 3D continuum [36]) is realized. In graphene a two-component scenario is realized as well, but within the very same 2D energy band. Our calculations indicate that, notwithstanding the damping, the graphene acoustic plasmon exhibits a spectral weight that is comparable to the spectral weight of the conventional 2D plasmon. As a consequence, the graphene acoustic plasmon discussed here should be accessible by high-resolution angle-resolved energy-loss (HREELS) experiments on extrinsic (doped) graphene. Our analysis suggests that such an acoustic plasmon might exist in other materials as well, as long as an anisotropic band is present near the Fermi level.

Acknowledgments

MP acknowledges the financial support of MIUR (FIRB-Futuro in Ricerca 2010—Project PLASMOGRAPH grant no. RBFR10M5BT), the European Commission, the European Social Fund and Regione Calabria, (POR) Calabria—FSE 2007/2013. VMS acknowledges financial support from the Spanish MICINN (no. FIS2010-19609-C02-01), the Departamento de Educación del Gobierno Vasco, and the University of the Basque Country (no. GIC07-IT-366-07).

References

[1] Novoselov K S, Geim A, Morozov S V, Jiang D, Zhang Y, Dubonos S V, Grigorieva I V and Firsov A A 2004 *Science* **306** 666
[2] Geim A K and Novoselov K S 2007 *Nature Mater.* **6** 183
[3] Castro Neto A H, Guinea F, Peres N M R, Novoselov K S and Geim A K 2009 *Rev. Mod. Phys.* **81** 109
[4] Bonaccorso F, Sun Z, Hasan T and Ferrari A C 2010 *Nat. Photon.* **4** 611
[5] Giovannetti G, Khomyakov P A, Brocks G, Karpan V M, van den Brink J and Kelly P J 2008 *Phys. Rev. Lett.* **101** 026803
[6] McChesney J L, Bostwick A, Ohta T, Seyller T, Horn K, González J and Rotenberg E 2010 *Phys. Rev. Lett.* **104** 136803
[7] Papagno M, Rusponi S, Sheverdyaeva P M, Vlaic S, Etzkorn M, Pacilè D, Moras P, Carbone C and Brune H 2012 *ACS Nano* **6** 199
[8] Liu Y, Willis R F, Emtsev K V and Seyller T 2008 *Phys. Rev.* B **78** 201403
[9] Tegenkamp C, Pfnür H, Langer T, Baringhaus J and Schumacher H W 2012 *J. Phys.: Condens. Matter* **23** 012001
[10] Shin S Y, Hwang C G, Sung S J, Kim N D, Kim H S and Chung J W 2011 *Phys. Rev.* B **83** 161403
[11] Chen J *et al* 2012 *Nature* **487** 77
[12] Fei Z *et al* 2012 *Nature* **487** 82
[13] Grigorenko A N, Polini M and Novoselov K S 2012 *Nat. Photon.* **6** 749
[14] Wunsch B, Stauber T, Sols F and Guinea F 2006 *New J. Phys.* **8** 318
[15] Hwang E H and Das Sarma S 2007 *Phys. Rev.* B **75** 205418
[16] Roslyak O, Gumbs G and Huang D 2011 *J. Appl. Phys.* **109** 113721
[17] Principi A, Asgari R and Polini M 2011 *Solid State Commun.* **151** 1627
[18] Yan J, Thygesen K S and Jacobsen K W 2011 *Phys. Rev. Lett.* **106** 146803
[19] Svintsov D, Vyurkov V, Yurchenko S, Otsuji T and Ryzhii V 2012 *J. Appl. Phys.* **111** 083715
[20] Kinyanjui M K, Kramberger C, Pichler T, Meyer J C, Wachsmuth P, Benner G and Kaiser U 2012 *Europhys. Lett.* **97** 57005
[21] Tomadin A and Polini M 2013 *Phys. Rev.* B **88** 205426
[22] Gao Y and Yuan Z 2011 *Solid State Commun.* **151** 1009
[23] Stauber T, Schliemann J and Peres N M R 2010 *Phys. Rev.* B **81** 085409
[24] Despoja V, Novko D, Dekanić K, Šunjić M and Marušić L 2013 *Phys. Rev.* B **87** 075447
[25] Pines D 1956 *Can. J. Phys.* **34** 1379
[26] Perdew J P and Zunger A 1981 *Phys. Rev.* B **23** 5048
[27] Troullier N and Martins J L 1991 *Phys. Rev.* B **43** 1993
[28] Monkhorst H J and Pack J D 1976 *Phys. Rev.* B **13** 5188
[29] Taft E A and Philipp H R 1965 *Phys. Rev.* **138** A197
[30] Kramberger C *et al* 2008 *Phys. Rev. Lett.* **100** 196803
[31] Hill A, Mikhailov S A and Ziegler K 2009 *Europhys. Lett.* **87** 27005
[32] Eberlein T, Bangert U, Nair R R, Jones R, Gass M, Bleloch A L, Novoselov K S, Geim A and Briddon P R 2008 *Phys. Rev.* B **77** 233406
[33] Ando T, Fowler A B and Stern F 1982 *Rev. Mod. Phys.* **54** 437
[34] Ashcroft N W and Mermin N D 1976 *Solid State Physics* (Philadelphia, PA: Hault Saunders)
[35] Pines D and Nozieres P 1989 *The Theory of Quantum Liquids* (New York: Addison-Wesley)
[36] Pitarke J M, Nazarov V U, Silkin V M, Chulkov E V, Zaremba E and Echenique P M 2004 *Phys. Rev.* B **70** 205403
[37] Silkin V M, García-Lekue A, Pitarke J M, Chulkov E V, Zaremba E and Echenique P M 2004 *Europhys. Lett.* **66** 260
[38] Diaconescu B *et al* 2007 *Nature* **448** 57

[39] Park S J and Palmer R E 2010 *Phys. Rev. Lett.* **105** 016801
[40] Pohl K, Diaconescu B, Vercelli G, Vattuine L, Silkin V M, Chulkov E V, Echenique P M and Rocca M 2010 *EPL* **90** 57006
[41] Vattuone L, Vercelli G, Smerieri M, Savio L and Rocca M 2012 *Plasmonics* **7** 323
[42] Yan J, Jacobsen K W and Thygesen K S 2012 *Phys. Rev.* B **86** 241404
[43] Jahn M, Müller M, Endlich M, Néel N, Kröger J, Chis V and Hellsing B 2012 *Phys. Rev.* B **86** 085453
[44] Vattuone L, Smerieri M, Langer T, Tegenkamp C, Pfnür H, Silkin V M, Chulkov E V, Echenique P M and Rocca M 2013 *Phys. Rev. Lett.* **110** 127405
[45] Pischel J, Welsch E, Skibbe O and Pucci A 2013 *J. Phys. Chem.* C **117** 26964